Macroscale Double Networks: Design Criteria for Optimizing Strength and Toughness

Daniel R. King[1,2,‡,*], *Tsuyoshi Okumura*[3,‡], *Riku Takahashi*[3,†], *Takayuki Kurokawa*[1,2], *Jian Ping Gong*[1,2,4*]

[1]Faculty of Advanced Life Science, Hokkaido University, Sapporo, 001-0021, Japan.

[2]Global Station for Soft Matter, Global Institution for Collaborative Research and Education, Hokkaido University, Sapporo, 001-0021, Japan.

[3]Graduate School of Life Science, Hokkaido University, Sapporo, 001-0021, Japan.

[4]Institute for Chemical Reaction Design and Discovery (WPI-ICReDD), Hokkaido University, Sapporo, 001-0021, Japan.

*Corresponding Authors: dking@sci.hokudai.ac.jp; gong@sci.hokudai.ac.jp

[†]Present Address: NTT Basic Research Laboratories, NTT Corporation, 3-1 Morinosato-Wakamiya, Atsugi, Kanagawa, 243-0198, Japan.

[‡]Author Contributions: These authors contributed equally.

KEYWORDS:

Double Network, Elastomer, Topological Interlocking, Toughness, Dissipation, Metamaterials

ABSTRACT

The double network concept, based on the fracture of sacrificial bonds, has been revolutionary toward the creation of robust soft materials. Based on the essence of double network hydrogels, macroscale, 3D printed rigid sacrificial networks are embedded within silicone rubber stretchable matrices. Preferential fracture of the sacrificial network results in a ~60 times increase in stiffness and a ~50% increase in work of extension compared to the neat matrix. Maximizing yield strength while maintaining multi-step internal fracture occurs when the strength of the sacrificial network approaches the strength of the matrix. Upon determining the optimal sacrificial network strength, the sacrificial bond section density can be increased to maximize energy dissipation, and toughening efficiencies up to ~70% of the maximum theoretical toughness are achieved. High toughness and dissipation are achieved because topological interlocking enables significant force transmission to the sacrificial network at smaller length-scales than interfacial adhesion, allowing much higher sacrificial bond density. This method is general and can be used with a variety of materials systems, without requiring strong interfacial adhesion, contrasting traditional composite systems. Demonstrating that the double network concept can be used at length-scales far beyond the molecular scale will have important implications toward the development of future structural materials.

1. INTRODUCTION

The development of unique toughening mechanisms has been important toward the deployment of hydrogel-based materials, because neat hydrogels exhibit poor mechanical properties compared to traditional soft materials such as rubbers.[1] For applications ranging from biomaterials[2,3] to soft electronics and robotics,[4–7] soft materials with improved mechanical

properties are required to bring these applications to reality. A variety of molecular mechanisms have been developed that allow traditionally brittle and weak materials to exhibit high strength, stretchability, and toughness. These mechanisms include slide-rings with mobile crosslinks,[8,9] healable dynamic bonds,[10–12] and double networks.[13–15] The double network concept requires an interpenetrating network design with strong contrasting structure and properties, where the "first network" consists of relatively short and stiff polymer strands, and the "second network" consists of relatively long and stretchable polymer strands (**Figure 1a**). Enhanced toughness is due to two effects: 1) when the sample is deformed, the covalent bonds of the first network fracture, dissipating energy, while the second network maintains global integrity, and 2) at the crack tip, the fracture of the first network softens the material to avoid stress concentrations, resulting in increased resistance to crack growth.[14] The double network concept has been extremely important toward modern hydrogel design as it enables gels that are tough but also have enhanced stiffness, similar to that of cartilage. Recently this mechanism has been developed and utilized in elastomeric materials as well, resulting in rubbers with unprecedented dissipation.[16,17] Structure modifications of traditional tires based on the double network concept has had commercial success in the automobile industry, and have recently been utilized in high performance eco-tires.

To develop useful soft materials, dissipation mechanisms that can be applied over a variety of time-scales and length-scales are required.[18] At relatively large length-scales this concept has proven successful by utilizing 3D printed structures[19–21], incorporating fibers,[22–26] and embedding liquid metals.[27–30] Analogous structures can be seen in biological materials.[31] For example, ligaments such as those in the human knee consist of stiff collagen fibers within a soft extracellular matrix,[32,33] and nacre consists of stiff ceramic plates held together by a soft protein-based cement.[34,35] Beyond simply increasing energy dissipation, these structures change the deformation

and fracture process by modifying how crack propagation occurs.[36] Creating composites by a similar design while utilizing recently developed advanced materials opens the possibility of creating stiff and tough soft materials that possess properties similar to, or beyond those seen in nature.

The success of the molecular-scale double network concept has led researchers to investigate whether the mechanism can be applied more broadly. Hong and coworkers developed the first "macroscale" double network composite, consisting of VHB tape adhered to a fabric mesh.[37] When stretched, the fabric mesh fractures, dissipating energy, while the viscoelastic tape prevents premature fracture of the sample. The stress on the composite is transmitted to the fabric through interfacial adhesion with the tape, and fracture of the composite occurs until small islands of fabric are formed, where the interface is not sufficiently strong enough to cause additional fracture. This method has been used as well in composite fibers with metal cores, which undergo multiple fracture events, increasing dissipation.[38,39] Inspired by the regularly folded structure of the biomacromolecule titin, Zhu et al. produced 3D printed soft composite structures with an incorporated thin and weak gel fiber sacrificial network.[40] When the gel fibers break, "hidden length" of gel is able to deform, dramatically improving the stretchability and toughness of the hydrogel composite. Recently, our laboratory created a hydrogel composite that dissipates energy at more than one length-scale.[41] On the molecular scale, a viscoelastic hybrid hydrogel was synthesized that exhibits high toughness and viscoelasticity due to strong hydrogen bonding between the monomer units. On the macroscale, a rigid frame was fabricated from a low melting point alloy (LMA). This composite exhibited the double network effect at millimeter length-scales, similar to the fracture process seen in the work by Hong and coworkers. When stretched, the LMA skeleton underwent multiple internal fracture events, acting as a sacrificial "first network." The

resulting mechanical properties for this composite include a stiffness comparable to the LMA skeleton, fracture strain comparable to the tough gel matrix, and a work of extension greater than the summation of the two independent phases. The macroscale double network (Macro-DN) mechanism enables unique mechanical properties in soft materials, which cannot be achieved by single materials alone.

While previous studies have recognized the importance of the double network effect in individual systems, the generalized design criteria for utilizing this mechanism in macroscale composites has not been elucidated. To carefully study the properties of Macro-DN composites, we utilize a combination of a 3D printed rigid plastic grid as a sacrificial "first network" reinforcing phase, embedded within a stretchable elastomer "second network" matrix consisting of a silicone rubber (**Figure 1b**). 3D printing allows for the easy design of first network structures (skeleton) with precision in all three dimensions. Elastomers possess properties that make them suitable as second networks, including simple preparation, high stretchability, and relatively high toughness. This model system provides a basis to systematically probe the parameter space of Macro-DN composites. Depending on the mechanical properties of the individual components, the composite system can exhibit multi-step internal fracture without global failure, resulting in high composite stiffness (from the reinforcing skeleton) and high stretchability (from the matrix). The hysteresis energy of these composites greatly exceeds that of the neat matrix. By tuning the strength of the reinforcing skeleton, we can control the yield force, defined for this system as the force at which sequential internal fracture occurs, creating a type of "mechanical fuse." We find that at a skeleton to matrix strength ratio of 1 the sample undergoes a transition from multi-step ductile to single-step brittle fracture, with optimal yield strength and toughness being achieved near the transition point. We also studied the force transmission mechanism and discovered that a grid-based skeleton that

results in topological interlocking is essential, as it enables force transmission at length-scales much less than can be achieved solely through interfacial adhesion. With this knowledge we were able to increase the sacrificial bond density significantly, resulting in a 51% increase in work of extension, and we ultimately reached a toughening efficiency of 71% of the theoretical maximum toughness. Without needing strong interfacial adhesion and using the mechanical guidelines introduced here, we were able to create tough composites with a wide range of material types, including renewable materials. Importantly, the Macro-DN method provides a pathway to incorporate important functional materials such as metals and ceramics into soft and ductile, yet tough composite structures. This work presents general design criteria for macroscale double network composites and should play an important role in expanding the mechanical properties of soft materials.

2. RESULTS AND DISCUSSION

2.1 Macroscale Double Networks

Rigid 3D printed grids are incorporated into a stretchable matrix as a sacrificial phase. These skeletons are designed to fracture, increasing energy dissipation in a manner analogous to the first network of double network gels. The use of 3D printing facilitates this process by allowing easy control of grid fracture strength, and has been shown to work well to incorporate soft materials.[40,42,43] The general design can be seen in **Figure 1c**, where the rigid skeleton is shown in dark blue, and the stretchable matrix is shown in light pink. Based on previous research that utilizes soft composite structures,[37,41] we can generally outline the role of each phase. The matrix controls the maximum fracture force, F_x, and stretch at break of the composite, λ_x, while the rigid skeleton controls the stiffness, k, of the composite. The vertical links within the rigid skeleton are designed to act as macroscale "sacrificial bonds." The force at which these bonds break, and their energy dissipation contribution, can be tuned by modifying the length, L_s, the cross-sectional area, A_{cs}, and

the number n_s, of the sacrificial bonds, or by changing the volume fraction, φ, of the matrix related to the rigid phase of the composite. Furthermore, the number of total sections, S, can be tuned, influencing the total potential cyclability, energy dissipation, and ductile response of the composite.

For the exemplary system, the reinforcing skeleton consists of a hard polyurethane-polyacrylate copolymer resin, with a modulus over 1 GPa, and the elastomer matrix is a commercial elastic silicone rubber with a modulus of approximately 1 MPa. The nominal dimensions are fixed, with a length of 34 mm, width of 12 mm, and thickness of 1.5 mm. The reinforcing grid contains $S = 9$ sections, each supported by three sacrificial bonds, $n_s = 3$. The thickness and width of the sacrificial bonds were 0.27 mm and 0.72 mm, respectively, resulting in total a cross-sectional area per section of $A_{cs} = 0.58$ mm^2 (complete detailed dimensions are shown in **Figure S1**). This sample has a volume fraction of matrix, φ, of 0.85. The force, F, versus stretch ratio, λ, for the skeleton, matrix, and Macro-DN composite can be seen in **Figure 1d** and **Table S1**. The two neat components have drastically contrasting mechanical properties in their independent form. The stiffness, k, of the skeleton (28.8 N/mm) is much greater than that of the matrix (0.51 N/mm), while the fracture stretch, λ_x, of the matrix (2.71) exceeds that of the skeleton (1.03). When combined, the mechanical properties of the composite are visibly different (**Video S1**). At small stretch, the composite is stiff and quickly fractures (**Figure 1d(i)**), eclipsing the curve of the neat skeleton. However, in contrast to the brittle failure of the independent skeleton, the force is transferred into the matrix, in the location of the initial fracture event (**Figure 1d(ii),** denoted by yellow dashed line). The decreased force and increased stretchability after fracture of the skeleton is similar in many ways to the release of "hidden length" in the protein titin.[40] As stretching continues, the force increases until the force in the matrix exceeds the fracture strength of the skeleton, and the skeleton fractures elsewhere, creating a second local deformation region (**Figure 1d(iii)**). This process

repeats (**Figure 1d(iv)**), and subsequent fracture events (**Figure 1d(v)** and **Figure 1d(vi)**) maintain the high force within the sample. Eventually, once all sacrificial bonds that make up the skeleton are fractured, rupture will occur through the matrix phase (**Figure 1d(vii)**).

The mechanical response of the macroscale composite can be analyzed by comparison to traditional double network hydrogels. The stiffness of the sample at small stretch is controlled by the stiffness of the skeleton (macroscale 1st network), resulting in an increase in stiffness of ~60. After fracture of this network, the composite undergoes yielding and enters a ductile region. In this

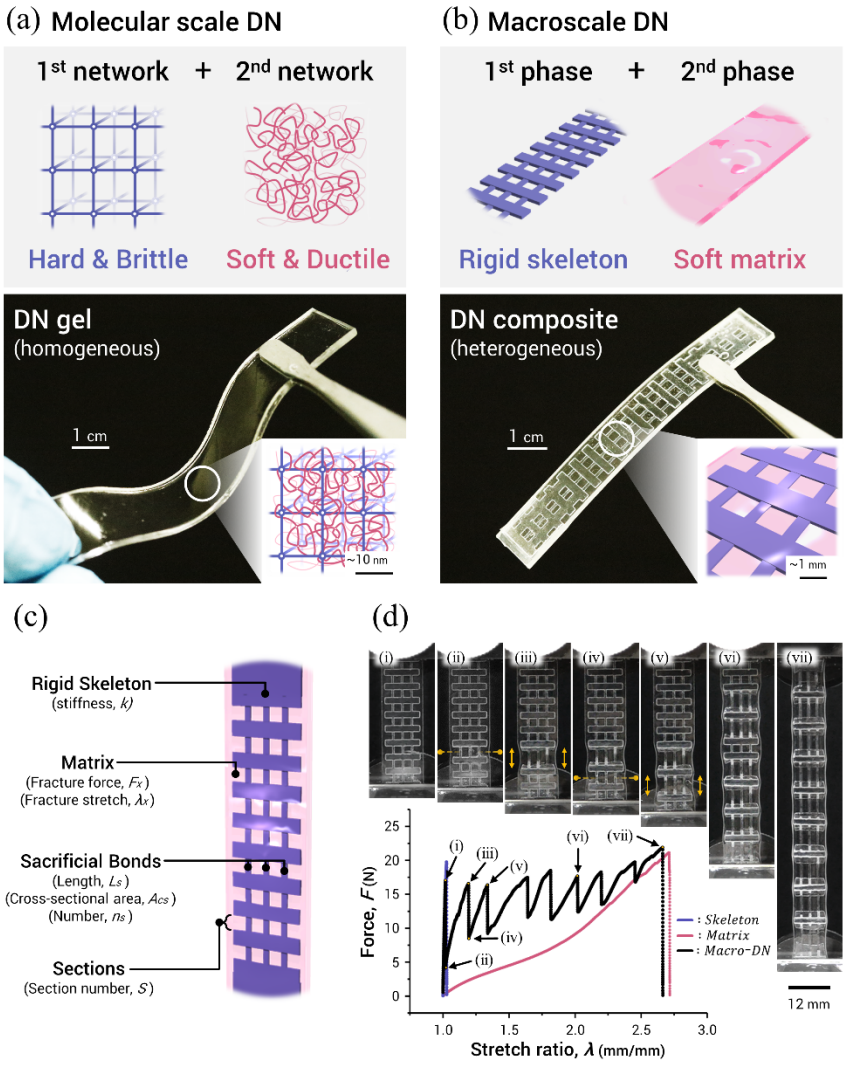

Figure 1. Extending the double network concept from the molecular scale to the macroscale. **(a)** Required network properties for creating double network materials: hard/brittle properties are required for the first network (sacrificial network) and soft/ductile properties are necessary for the 2nd network. **(b)** Implementation of the double network concept on the macroscale. The Macro-DN composite has a first phase consisting of a 3D printed, rigid grid, and a soft silicone rubber second phase. **(c)** Schematic of a Macro-DN composite. Features are listed with their specific design parameters. **(d)** Force-stretch curves of a grid-shaped skeleton (purple), neat silicone rubber (pink), and their resulting Macro-DN composite (black). The insets (i)-(vii) represent snapshots of the composite sample corresponding to the stretch shown in the loading curve. Yellow dashed lines represent internal fracture events and local deformation.

region, ranging in stretch from about 1.2 to 2.5, The average force is 14.8 ± 2.5 N, with the force oscillating between a relative minimum (relaxation after a fracture event) and relative maximum (prior to fracture of the skeleton). In the ductile region, the sample experiences permanent fracture of the first network as a function of stretch. Once the entirety of the sample has undergone necking, the sample will fracture through the matrix (macroscale 2nd network). This fracture event occurs near the same stretch as that of the independently tested matrix component ($\lambda_x \sim 2.7$). **Table S1** contains the complete mechanical properties of the skeleton (1st network), matrix (2nd network), and Macro-DN composite.

We can analyze the energy dissipated of each phase by integrating the area under the force versus displacement curves to determine the work of extension, *W*. During stretching of the skeleton in **Figure 1d**, 11 mJ of energy is dissipated due to the fracture of 3 sacrificial bonds that make up one section. Fracture of the neat matrix required 530 mJ, and the energy required to fracture the composite structure was 850 mJ. Given that each section of the frame underwent fracture in the composite, a total of 9 sections containing 27 sacrificial bonds fractured, requiring ~100 mJ of energy. However, we can see that the resulting composite required 250 mJ more energy than the simple sum of the sacrificial bond energy plus the stretching of the matrix, demonstrating a synergistic increase in the toughness of the composite structure. The increase in toughness of these composites is not limited to just the addition of sacrificial bonds that dissipate energy when they break; the fracture process itself increases the dissipation of the matrix as well due to localized large deformation of the matrix in the fractured section. This matches the response of double network hydrogels, where the introduction of the first brittle network dissipates energy not only by fracturing covalent bonds, but also by supporting large local deformation of the second network in regions where first network fracture occurs. A similar process is shown here: only a minority of the

energy dissipated can be attributed to fracturing of the sacrificial network, and we therefore conclude that the presence of the sacrificial network also increases the dissipation in the silicone rubber matrix.

Another unique feature of double network hydrogels is that they exhibit significant hysteresis during cycling due to fracture of the sacrificial first network.[44] **Figure 2** demonstrates cycle testing with increasing stretch for Macro-DN composites. **Figure 2a** demonstrates cyclic testing of the neat silicone rubber component, while **Figure 2b** charts the energy dissipated during each cycle. Hysteresis energy is calculated by the difference in the loading energy and the unloading energy. At small λ, the material exhibits strongly elastic properties, with loading and unloading curves virtually overlapping. As λ increases, the amount of energy dissipated increases, likely due to friction between polymer chains, or the onset of chain fracture due to finite extensibility of the network. These results are drastically different than those seen in the cyclic tests of the Macro-DN sample, shown in **Figure 2c**. Initially, the sample is very stiff, and when the force surpasses about 15 N, fracture of the reinforcing skeleton occurs. This fracture process causes the elastomer in the activated section to stretch, while the remaining sections keep their initial geometry. Interestingly, as presented in **Figure 2d**, the energy dissipated in the 2nd cycle (~100 mJ) of the Macro-DN composite exceeded that of the final, largest applied stretch of the neat rubber (~85 mJ). In other words, the composite dissipated as much energy at $\lambda = 1.2$ as the neat elastomer dissipated at nearly $\lambda = 2.6$. Neat silicone rubber only dissipates significant energy at high λ, close to λ_x. Due to localized stretching from the Macro-DN architecture, high *local* stretch is achieved at low *global* stretch. This design results in a material that is capable of dissipating large amounts of energy, even at small stretches, through fracture of a sacrificial network which controls local deformation.

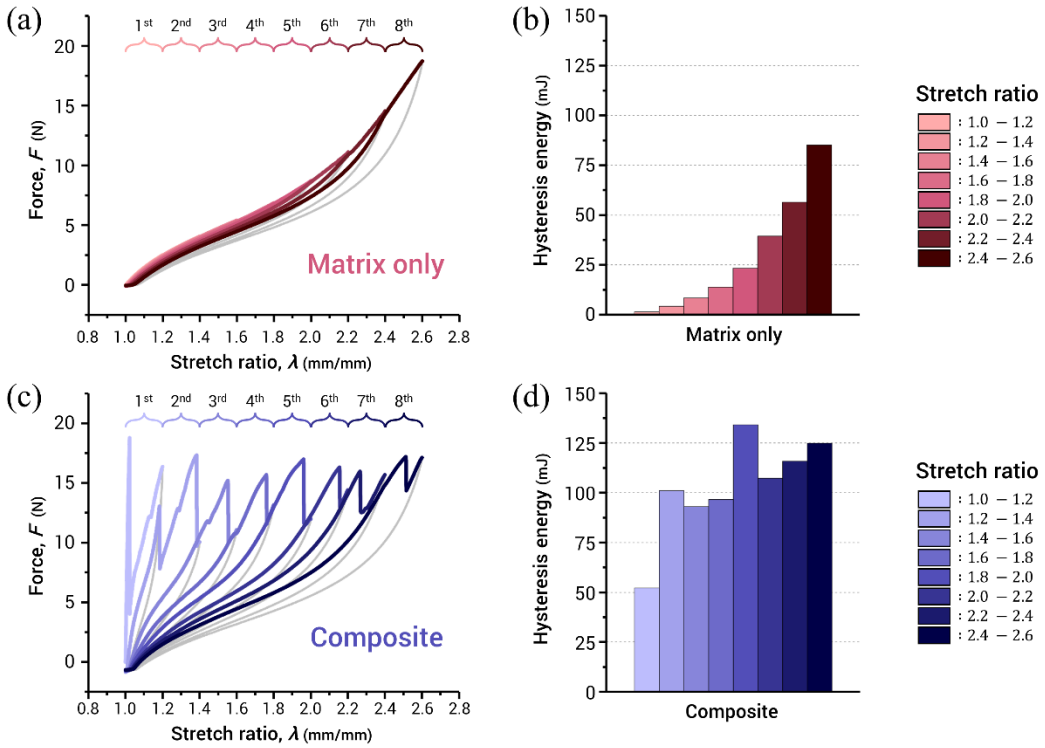

Figure 2. Analyzing energy dissipation via cyclic testing of the matrix and Macro-DN composite. Force versus stretch ratio curves during cyclic testing with repeatedly increasing stretch, and the hysteresis energy during each cycle are shown for the matrix (**(a)** and **(b)**, respectively) and Macro-DN composite (**(c)** and **(d)**, respectively). The neat matrix does not dissipate large energy until high stretch. The Macro-DN composite dissipates large amounts of energy, even at small stretch due to preferential fracture of the macroscale sacrificial network.

Interestingly, during the cyclic loading curves in **Figure 2c,** the force never exceeded a value of approximately 18 N. As the force approaches this value with the addition of stretch, the rigid grid will fracture, causing a decrease in force. The Macro-DN composite design acts like a "mechanical fuse." For these materials, if the force applied exceeds a given force determined by the grid design, fracture and additional displacement will occur, rather than an increase in force. This could be a useful design for shock sensitive applications, whereby tuning the mechanical properties of the composite can allow for programmable maximum force values within a given displacement range.

2.2 Enabling Multi-Step Fracture through Optimized Component Strength

In double network hydrogels, the yield stress is controlled by the properties of the first network,[45] and similarly we can control the yield force of Macro-DN composites by tuning the strength of the reinforcing skeleton. To change the fracture force, F_x, of the grid, we changed the nominal width of the sacrificial bonds of the skeleton structure from 0.45 mm to 1.2 mm, which resulted in cross-sectional areas, A_{cs}, ranging from 0.26 mm^2 to 1.04 mm^2 per section (**Figure 3a,** grid specifications are shown in **Table S2**). As A_{cs} increases, F_x increases proportionally (**Figure S2**). The force versus stretch curves for composites made with these skeletons can be seen in **Figure 3b**, along with an inset of the low stretch region in **Figure S3**. For the sample with the weakest sacrificial bonds, a ductile response with a sawtooth fracture pattern can be seen from a stretch of 1.0 to 1.5, and the nine peaks demonstrate complete fracture of all sacrificial bonds. After the bonds are completely fractured, the stress increases in the remaining intact matrix, until global fracture occurs at a stretch of about 2.75, matching λ_x of the silicone rubber matrix (**Figure 1d**). As the fracture strength of the incorporated skeleton increases, two noticeable changes occur, which are outlined in **Figure 3c**. First, the average F_x during rupture of the sacrificial bonds increases (internal fracture events denoted as circles and the average force as a dotted line). This occurs because the higher strength of the sacrificial network requires more force to fracture. Second, the stretch range over which sacrificial bond fracture occurs increases with increasing strength, until the A_{cs} = 0.58 mm^2 sample, where sacrificial bond fracture occurs until matrix rupture (denoted as an *X* in **Figure 3c**). Stiffer skeletons require higher force to fracture, and therefore greater stretch between fracture events is required. When the width of the grid is further increased (A_{cs} = 0.83, 1.04 mm^2), only one fracture event occurs, resulting in highly brittle composites with reduced fracture stretch. The optimized skeleton geometry for samples of this size were determined to have a sacrificial network

with A_{cs} = 0.58 mm^2, resulting in a composite with high stiffness and high toughness, while maintaining ductile characteristics.

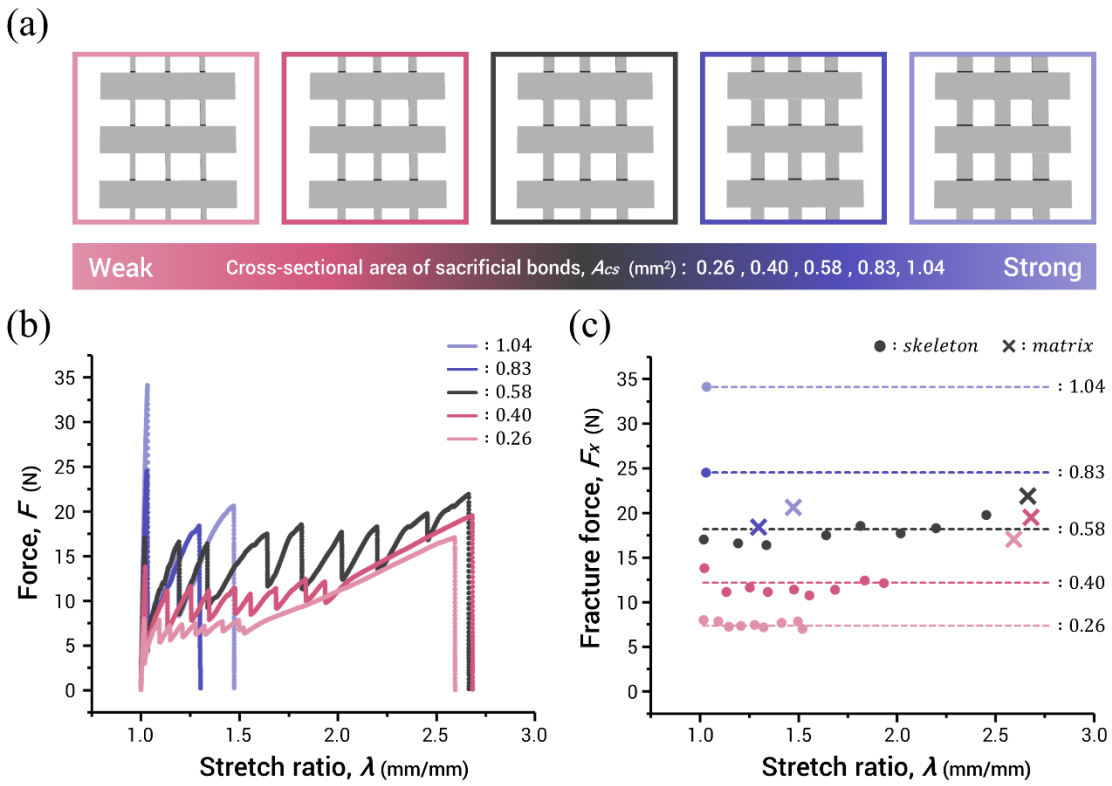

Figure 3. Tuning the mechanical response of Macro-DN composites by modifying the geometry of the sacrificial skeleton. **(a)** Schematic illustrations of the tested geometries of grid-shaped skeletons used in the Macro-DN composites. **(b)** Typical force versus stretch curves of the composites with varying geometry of skeletons. The legend values are the cross-sectional area per section of vertical grid. **(c)** Fracture forces measured during a tensile test, either due to skeleton fracture (circle) or matrix fracture (cross). Fracture of the matrix occurred when the sample failed.

A powerful result of multi-step internal fracture is that Macro-DN composites are able to overcome weaknesses in the reinforcing skeleton. **Figure 4** demonstrates a sample where the grid sections contain varying A_{cs}, from 0.26 mm^2 to 1.04 mm^2. When stretched, fracture occurs first in the sections with A_{cs} = 0.26 mm^2. However, rather than failing at F_x = 8 N (denoted by the pink line, the fracture force of the A_{cs} = 0.26 mm^2 skeleton), force is transmitted to the matrix, allowing the next stiffer sections to fracture. This process continues until matrix rupture. Since the fracture force of the A_{cs} = 0.83 mm^2 and 1.04 mm^2 sections exceeds that of the matrix, they cannot fracture,

and λ_x occurs at reduced stretch. Multi-step internal fracture results in materials that are flaw-resistant and can overcome defects. Furthermore, by tuning A_{cs}, we have a method to tune the shape of the loading curve, especially useful in biomaterials where "J-shaped" curves are desired.[46]

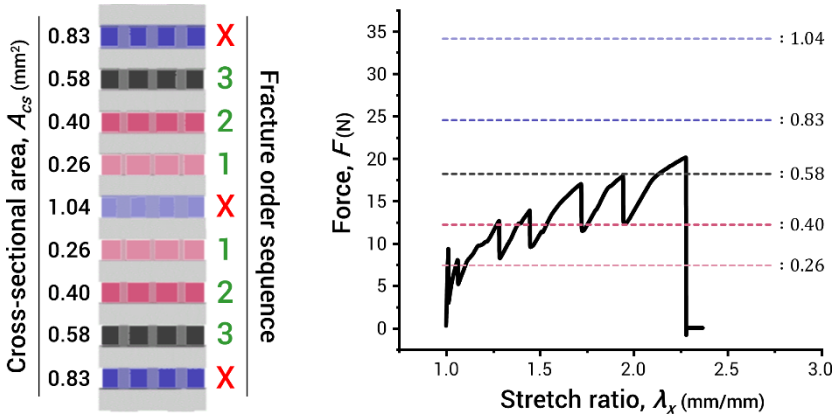

Figure 4. Force versus stretch ratio curve for a Macro-DN composite containing sections with varying cross-sectional area, A_{cs}, as shown on the left. Colored lines on the plot represent the fracture force for sections of corresponding A_{cs}. The weakest sections fracture first, followed by stronger sections, as denoted by the fracture order sequence. Sufficient force is not generated to fracture some sections (A_{cs} = 0.83 mm^2, 1.04 mm^2), denoted by a red X.

To understand the ductile-brittle transition, we compared the observed fracture behavior of the composites to the mechanical strength of the reinforcing skeleton. In **Figure 5a**, the strength of grids with varying A_{cs} are plotted (symbols), along with the strength of the silicone rubber matrix (green line). When the fracture force of the matrix exceeds the fracture force of the skeleton, multi-step internal fracture occurs (pink symbols) whereas when the fracture force of the skeleton is greater than the matrix, only single-step fracture occurs (blue symbols). If we examine the samples at the moment prior to fracture (**Figure 5a** insets), we see that the samples that underwent multi-step internal fracture were dramatically deformed and all sacrificial bonds were broken, while the single-step internal fracture samples have only one cracked region, lacking global damage. Based on these qualitative results, we conclude that the defining feature of macroscale double networks

is multi-step internal fracture, which occurs when the fracture strength of the matrix exceeds that of the reinforcing skeleton grid.

From the photographs in **Figure 5a**, we see that multi-step internal fracture allows for higher λ_x than single-step internal fracture. These results are quantified in **Figure 5b**. In the multi-step (pink) region, λ_x approaches 2.75, but when the grid to matrix strength ratio goes above 1, λ_x dramatically decreases to below 1.5 (blue region). In **Figure 5c**, we plot the work of extension, W, of the composite samples, which was calculated by integrating the force versus displacement curve. When weak skeletons are used, there is little change in the overall W. The introduction of a weak grid does not dramatically increase the force during stretching but may consequently introduce defects within the matrix to nucleate fracture. W reaches a maximum when the skeleton to matrix strength ratio approached 1. If the grid strength to matrix strength is further increased, W dramatically drops, because the matrix is unable to deform to dissipate energy. These results show that the ratio of skeleton strength to matrix strength is the key factor governing the ductile-brittle

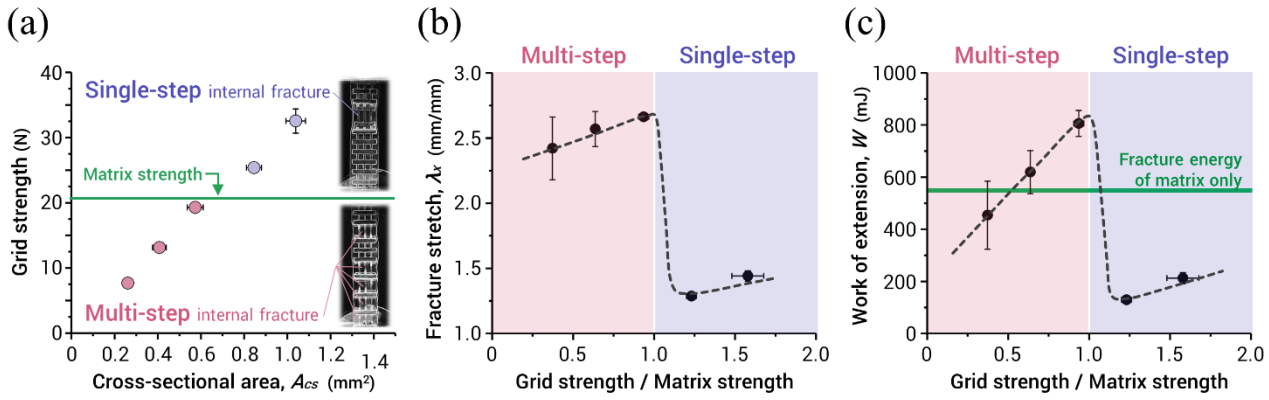

Figure 5. Ductile-brittle phase transition of the Macro-DN composites. **(a)** Fracture strength versus cross-sectional area for the 3D printed grid and the silicone rubber matrix. The insets represent images of multi-step and single-step internal fracture. **(b)** Stretch-at-break versus the grid to matrix strength ratio for the composite samples. A transition occurs when the strength ratios reach 1. **(c)** Work of extension versus the grid to matrix strength ratio. The highest work of extension occurs at a grid to matrix strength of 1. Tests were performed at least 5 times, and error bars represent standard deviation. Data points without error bars have error less than the symbol size.

transition of the double network composites, and that the optimization point for stretchability and energy dissipation lies at a ratio of one.

2.3 Maximizing Force Transmission with Topological Interlocking

Usually, the interface between the reinforcing phase and the matrix plays an important role in composite materials. This is especially true in macroscale composites or laminated structures, where delamination can quickly result in composite failure. In previous work on Macro-DN composites based on fabric and VHB tape, force transmission occurred primarily due to adhesion between the two phases.[37] As the sample stretched, the fabric fractured and the magnitude of force transmitted from the rubber to the fabric continuously diminished. At some point, the force transmitted was not great enough to fracture the fabric, and this was followed by rupture of the VHB tape matrix. In our experiments, a grid shape was chosen because it allows for the transmission of force between the matrix and skeleton via topological interlocking as well as by interfacial adhesion, resulting in a composite that does not easily delaminate. Understanding the roles of interfacial adhesion and topological interlocking is important toward optimizing the design of macroscale double network structures.

To understand the role of interfacial adhesion, we designed an experiment to measure the adhesive strength between the silicone rubber and the skeleton (**Figure 6a**). A rigid rod of 3D printed plastic was embedded in silicone rubber with lengths of 5, 7, 10, and 16 mm, with a constant A_{cs} of 0.4 mm^2. The silicone rubber was clamped with the bottom grip of the tensile tester, and the rod was displaced at 50 mm/min. The force versus displacement curve can be seen in **Figure 6b**. The force increased, until slipping occurred and then the force dropped nearly to 0 N as the rod was pulled out of the rubber. From the peak force, we normalized by the surface area of the rod to determine the maximum adhesion strength. The average adhesive shear stress, σ_a, of the four

lengths tested was 0.24 MPa (**Figure 6c**). This stress is exerted by the matrix on the skeleton, and therefore specimens with longer sacrificial bond lengths are expected to reach higher force in the skeleton during stretching. The force applied to the skeleton, F_s, can be calculated as:

$$F_s = L_s P_s n_s \sigma_a$$

where L_s is the sacrificial bond length, P_s is sacrificial bond perimeter, and n_s is total number of sacrificial bonds. For a fixed P_s (1.98 mm) and n_s (3), and using σ_a as calculated above, F_s is estimated as a function of sacrificial bond length in **Figure 6d**. The strength of the skeleton was experimentally measured as 16 N. From the plot in **Figure 6d**, the adhesion force exceeds this

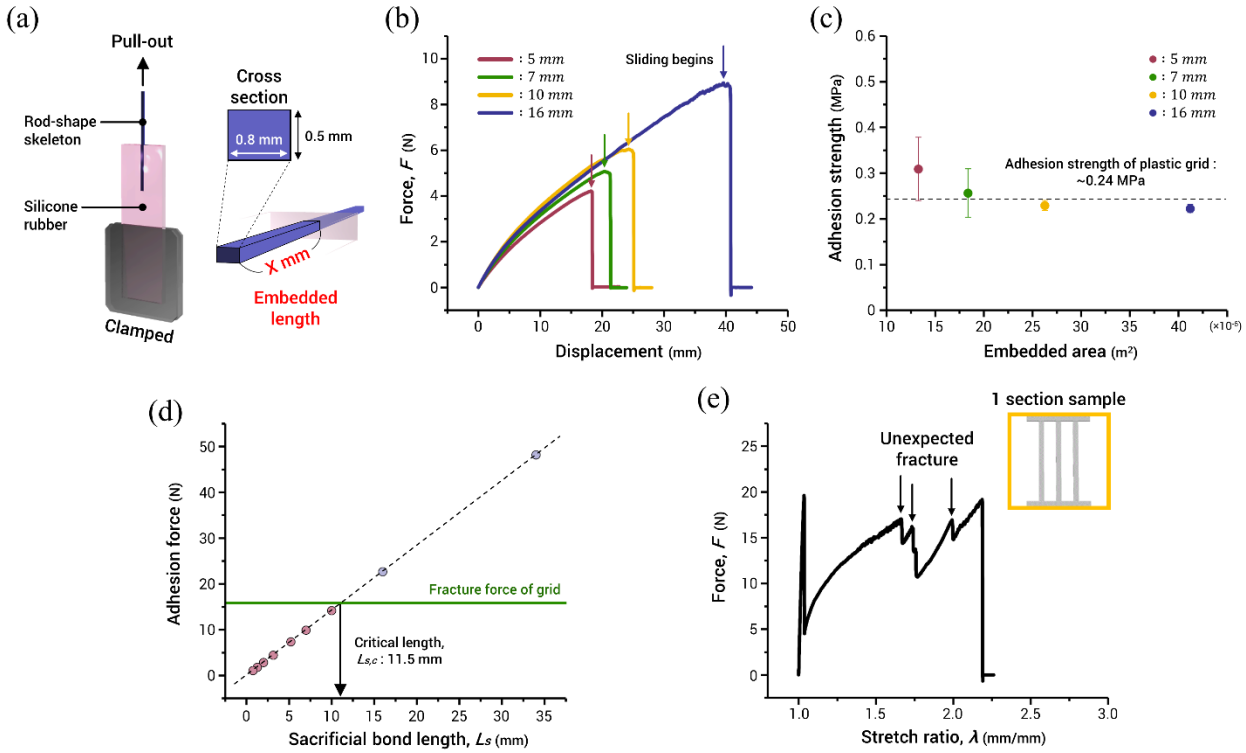

Figure 6. Investigation of adhesion strength between the 3D printed skeleton and silicone rubber. **(a)** Schematic of the test setup used to determine the adhesion strength between the silicone rubber and the 3D printed plastic. A rigid rod of length, *x*, was embedded in silicone rubber, and both the silicone rubber and the rod were gripped by opposing ends of a tensile tester. Displacement occurred at a rate of 50 mm/min. **(b)** Force versus displacement curves for rods of varying embedded length. Once the rod began to slide the force dropped to nearly 0 N and the test was ended. **(c)** Measured adhesion strength as a function of embedded surface area. **(d)** Calculated adhesion force, as a function of sacrificial bond length for grid sections containing a sacrificial bond cross section of 0.58 mm^2. The critical length of 11.5 mm represents the transition between fracture due to interfacial adhesion and topological interlocking. **(e)** Force versus stretch ratio curve for a sample containing only one section. Multiple fracture events are seen, due to the sufficiently strong adhesion force between the skeleton and the matrix.

value at a critical length, $L_{s,c} \sim 11.5$ mm. If the sacrificial bond length is greater than this value, multiple fracture events can occur within one sacrificial grid section due to adhesive force transfer. To test this claim, a sample was prepared with only one section ($S = 1$), containing sacrificial bonds with $L_s = 34$ mm (**Figure 6e**). In this sample, force can only be transmitted by interfacial adhesion. Upon close examination of the tensile tests for this specimen, we see that the initial fracture of the sacrificial network occurs at low stretch, immediately after the test begins. After this the force drops, but begins to increase again, and at above $\lambda = 1.5$, additional fracture events occurred within the already fractured section, due to adhesive force transmission. However, after three fracture events no additional internal fracture occurred and the sample failed globally. This starkly contrasts the fracture process of the specimen tested in **Figure 1d**, where a sample of identical length contained $S = 9$ sections and underwent nine fracture events. Despite possessing very short sacrificial bonds ($L_s = 2$ mm), multi-step fracture could occur because force was transmitted by the interlocking design. Because the adhesion between the matrix and skeleton is relatively weak, the impact of changing the number of bonds per section, n_s, is negligible. In **Figure S4**, we demonstrate that when $n_s = 5$ without changing A_{cs} the resulting $L_{s,c}$ decreases slightly to 9.7 mm. For the highest performance sample where L_s is very short, force transfer still occurs due to topological interlocking. These results clearly demonstrate the importance of a design that enables topological interlocking, since fracture can occur even when adhesion force between phases is low.

Next, we wanted to optimize energy dissipation by increasing the total number of fracture events. Samples with varying section number, S, from 0 (neat matrix) to 13 were fabricated. Since nominal length is fixed, when S increases, L_s must correspondingly decrease (**Table 1**). The force versus stretch ratio curves for representative specimens are shown in **Figure 7a**. As the L_s decreases and S increases, the frequency of the sawtooth pattern during yielding also increases, but λ_x does

not significantly change. With decreasing L_s, the local stretch per given displacement increases, causing the force to rise quickly and more fracture events occur within the same total displacement. This causes the average force during the yielding region to increase, consequently resulting in increased energy dissipation.

For a simple elastomer, the force-displacement curve takes on a generally triangular shape, and the work of extension can be approximated as $W_0 = 0.5*F_x*\delta_x$. We envision that the force versus stretch curve for a "perfect" Macro-DN composite would be a square shape (**Figure 7a**, bottom). To achieve this shape, stiff reinforcement is needed to quickly achieve a loading force

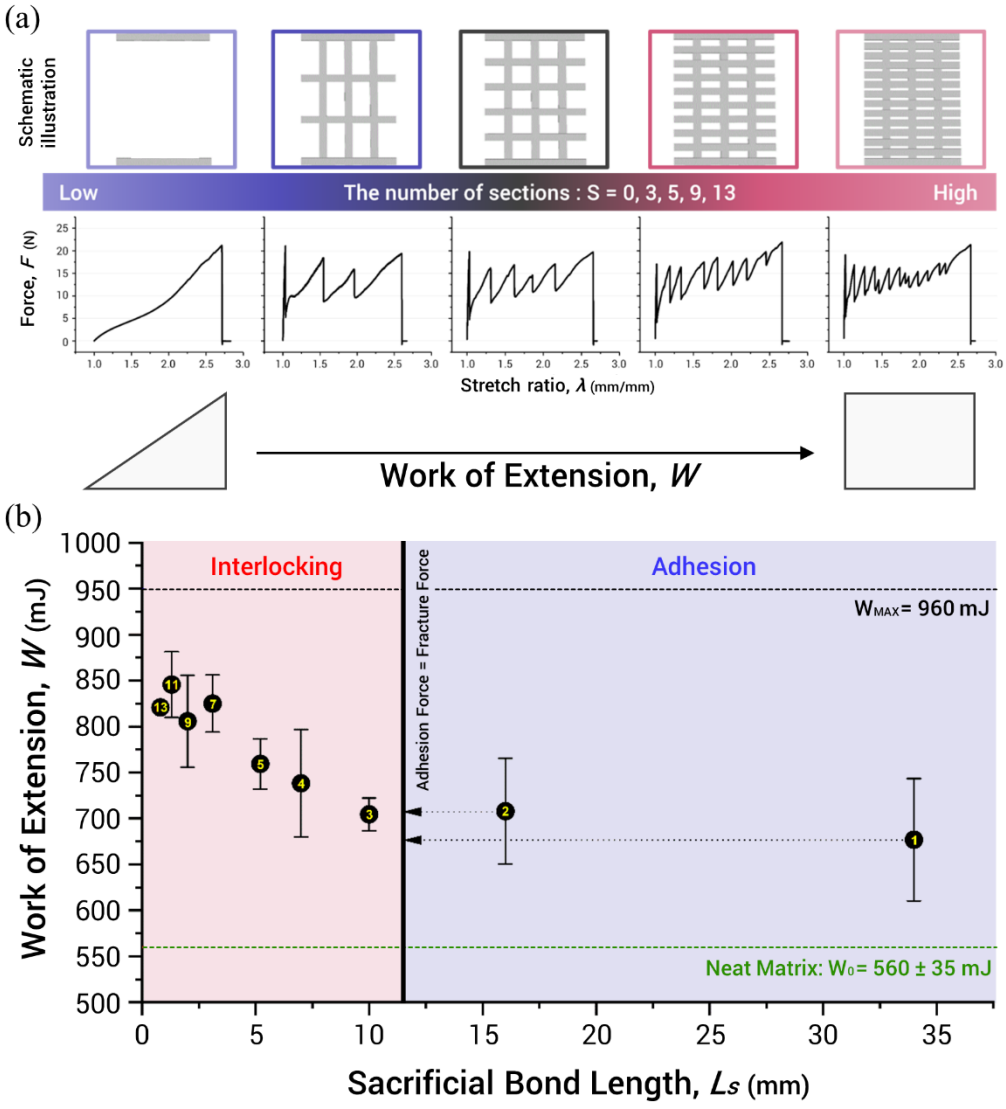

Figure 7. Effect of grid density on the toughness of Macro-DN composites. **(a)** The number of sections, *S*, was increased from 0 to 13. Schematics of these designs are shown with representative force versus stretch ratio curves. As the density of sacrificial bonds increases, the shape of the curve changes from a triangle to a rectangle, with nominally the same stretch ratio, representing an approximate doubling of the work of extension. **(b)** The work of extension as a function sacrificial bond length. The black line represents the transition in the dominant force transmission mechanism: at short sacrificial bond lengths topological interlocking plays is essential, and at long sacrificial bond lengths interfacial adhesion is important. The numbers in the symbols are the number of sections, *S*. The green dashed lined represents the work of extension of the neat matrix. The black dashed line represents the maximum work of extension, calculated from the skeleton fracture force and elastomer maximum stretch.

near the fracture strength of the matrix. Fracture should occur quickly and repeatedly, so that the average force during the yielding region remains close to the maximum yield strength. Finally, fracture should occur at the same stretch-at-break as the neat matrix. This fracture process would then approach a value of $W_{max} = F_{yield}*\delta_x$, where F_{yield} is the average peak force in the yielding region. In Section 2.2, we characterized the important factors in maximizing yield force, and in an optimized state $F_{yield} = F_x$ for a given matrix. Based on this model for a linear elastic matrix, we predict a 100% increase in work of extension is likely an upper bound for this type of composite system.

Table 1. Details of the properties of composites made with varying number of sections containing sacrificial bonds.

Number of Sacrificial Sections for a constant sample length, *S*	Number of Fracture Events	Bond Length, L_s (mm)	Matrix Volume Fraction, φ	Work of Extension, W (mJ)	Increase in Work of Extension*, $(W-W_0)/W_0$	Toughening Efficiency*, $(W-W_0)/(W_{max}-W_0)$
1	3	34.0	0.96	680 ± 67	21%	29%
2	3	16.0	0.95	710 ± 58	26%	37%
3	3	10.0	0.93	700 ± 18	26%	36%
4	4	7.0	0.92	740 ± 59	32%	44%
5	5	5.2	0.90	760 ± 27	36%	50%
7	7	3.1	0.88	830 ± 31	47%	66%
9	9	2.0	0.85	810 ± 50	44%	61%
11	11	1.3	0.82	850 ± 36	51%	71%
13	13	0.8	0.79	820 ± 6	47%	65%

*: $W_0 = 560$ mJ is the work of extension of neat matrix, $W_{max} = F_{yield}*\delta_x = 960$ mJ.

In **Figure 7b**, the work of extension, W, versus the sacrificial bond length, L_s, is plotted, with the number of sections, S, inscribed within each symbol. The green dashed line represents W of the neat matrix, W_0 = 560 mJ. The vertical black line at 11.5 mm represents the critical sacrificial bond length $L_{s,c}$ at which the adhesion force equals the fracture force of the skeleton. When L_s is greater than or near $L_{s,c}$, fracture occurs independently of section number; hence, samples with 1-3 sections exhibit similar W. When L_s is less than $L_{s,c}$, each section exhibits only one fracture event, due to topological interlocking, and as L_s decreases and S increases, more energy is dissipated. We ultimately measured a maximum work of extension of W = 850 mJ, in a sample containing S = 11 with L_s = 1.3 mm. This result represents a 51% increase in W compared to the W_0, due to the implementation of macroscale sacrificial bonds with topological interlocking. When samples where force transmission occurs by primarily by interfacial adhesion (1-3 section samples), the average increase in W is only 24%. These results demonstrate the importance of topological interlocking in creating robust Macro-DN composites.

We estimate that the maximum theoretical work of extension for this system can be calculated from F_{yield} = 16 N and δ_x = 60 mm ($\delta_x = initial\ length * \lambda_x$), resulting in W_{max} = 960 mJ (black dashed line in **Figure 7b**). To calculate the toughening efficiency, we compared the true increase in work of extension ($W - W_0$) to the maximum potential increase in work of extension ($W_{max} - W_0$). The results are tabulated in **Table 1.** When S = 11, the highest toughening efficiency, 71%, was measured. Interestingly, even with optimized grid strength, when S = 1 a toughening efficiency of just 29% was observed. There are a few reasons why a toughening efficiency of 100% was not achieved. The calculation of W_{max} assumes that there is no decrease in force between the fracture of subsequent sections; effectively the calculation assumes an infinite number of fracture events, which causes F_{yield} to be maintained for the duration of the yielding region. Furthermore, it

assumes that the force will not increase after all the sacrificial sections are activated. Finally, as *S* increases the volume fraction of matrix, φ, decreases (see **Table 1**). A detailed analysis of the specific contributions to energy dissipation in this system will be discussed in a subsequent report.

Previous work agrees with our finding that to make robust composites, topological interlocking is essential. Experiments performed on molecular-scale double networks, have shown that strong intermolecular interactions are not required to create double network structures; topological interlocking is sufficient to dramatically enhance mechanical properties via the interpenetrated double network structure. Furthermore, gels and elastomers can achieve strong bonding through topology at either the molecular-scale[47–49] or macroscale.[50] Ultimately, we see in Macro-DN systems that the incorporation of topological interlocking at large length scales also results in a dramatic increase in material toughness. Importantly, force transmission by topological interlocking makes developing Macro-DN composites using various soft and hard materials possible.

2.4 Universal Application of Macroscale Double Networks

Specific materials chemistry is not required to create Macro-DN composites; as long as the guiding mechanical parameters are followed, specifically that the fracture strength of the matrix exceeds the strength of the reinforcement and the design incorporates topological interlocking, components consisting of any type of material can be used. **Figure 8** contains examples that demonstrate the universality of this concept. **Figure 8a (**wood) and **Figure 8b** (foamed polystyrene; Styrofoam) demonstrate two other materials used as reinforcing phases within a silicone rubber matrix. In both cases the toughness increases along with the introduction of yielding, without influencing λ_x. For the Styrofoam sample, the irregular foamed structure likely causes additional fracture events to occur at smaller length-scales, due to increased topological interlocking, which prevents the immediate stress relaxation and significant saw-tooth pattern seen with other material combinations. In **Figure 8c**, natural rubber is used as a matrix. After the yield point, when the force

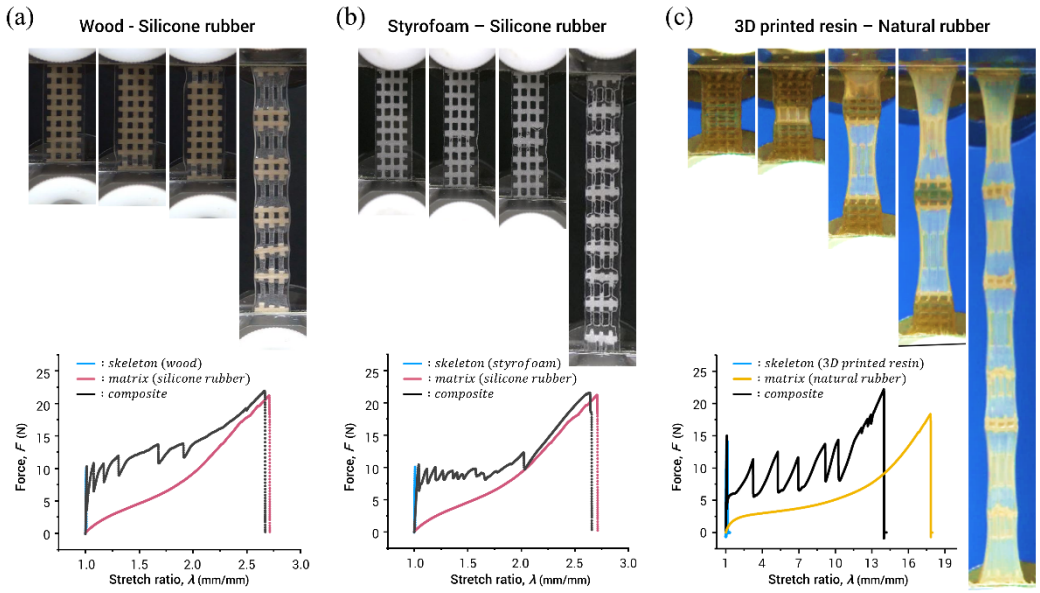

Figure 8. Demonstrating the universality of the macroscale double network effect by creating composites with a wide range of materials. **(a)** A composite comprised of wood and silicone rubber. **(b)** A composite comprised of Styrofoam and silicone rubber. This design lacks the obvious sawtooth fracture pattern of other designs, likely due to stronger topological interlocking due to the foamed structure. **(c)** A composite comprised of a 3D printed grid and natural rubber.

begins to rebuild, the slope has positive concavity, compared to the linear slope seen in silicone rubber samples. At high stretch, natural rubber exhibits significant strain hardening. During each internal fracture event, the rubber locally stretches to high strain, and therefore during each fracture event strain hardening is apparent. This opens up the possibility that this design could be used to create high performance materials by locally taking advantage of viscoelastic behaviors of designer polymers. Natural rubber is one of the toughest soft materials known, and generally represents an upper bound of toughness through intrinsic toughening. This method demonstrates that even the toughness of natural rubber can be improved by using a macroscale double network design. The use of metals as a sacrificial phase has been previously demonstrated,[38,39,41] and the use of ceramics in the sacrificial phase has strong potential due to their high stiffness and brittleness. We expect that Macro-DN composites containing metals and ceramics to play an important role in future functional materials designs. For materials that demand high energy dissipation, the macroscale double network method may universally enable higher performance with relatively minor changes in bulk materials.

3. CONCLUSION

Enhanced toughness can be achieved in soft composite structures by following design principles extrapolated from our knowledge of double network hydrogels and elastomers. Specifically, these composites are designed by integrating a rigid skeleton with high strength but a relatively low fracture force into a stretchable matrix. When stretched, force from the matrix causes the skeleton to fracture multiple times prior to global sample fracture. This matches the fracture mechanism inferred from double network gels, where a stretchable second network causes the brittle first network to fracture, resulting in yielding prior to global fracture. We have shown that the strength ratio between the skeleton and matrix governs multi-step, ductile versus single-step,

brittle deformation. As the strength of the skeleton approaches that of the matrix, the yield force reaches a maximum, and the yielding region extends in length, close to the ultimate fracture stretch of the composite, resulting in an optimized design. By studying the force transmission mechanisms, we determined that topological interlocking is essential. Utilizing topological interlocking, a significant increase in sacrificial bond density is achieved, reaching ~70% of the theoretical maximum toughness, compared to ~30% for the adhesion-only compositions. This mechanism also matches double network hydrogels, where topological interpenetration is more important than inter-network interactions. Because topological interlocking of the two phases provides sufficient force transmission, we demonstrate that the macroscale double network design is universal, and can be applied to wide range of materials, even if interfacial adhesion strength is poor. In the future we hope to leverage this model toward improving and designing double network hydrogels at all length-scales.

4. EXPERIMENTAL

4.1 Materials

The silicone elastomer used as the matrix is a commercially available two-part kit, KE-1603-A and KE-1603-B, (Shin-Etsu Chemical) and was used as received and according to instructions. Additionally, natural rubber (Qua Yu Kasei) was used as a matrix material in section 2.4. The materials required to fabricate the rigid grid are AR-M2 (model material) and AR-S1 (support material) and were purchased from Keyence Co. AR-M2 consists of acrylate monomer, urethane-acrylate oligomer and photoinitiator. AR-S1 consists of acrylate monomer, polypropylene glycol and photoinitiator. Additional grids were made with wood (TOKYU HANDS), and Styrofoam (TOKYU HANDS) in section 2.4.

4.2 Fabrication of the plastic skeleton

The grid-shaped plastic skeletons were 3D printed (AGILISTA-3000, Keyence). 3D printing allows for easy design via computer-aided drawing software and provides fine control over geometry as well as good reproducibility. A spacer was printed around the exterior of the grid to maintain a total composite thickness of 1.5 mm and was removed prior to sample testing. The specific geometric parameters which were varied include the number of sections (from 1-13) and the cross-sectional area of the sacrificial bonds (designed thickness of 0.3 mm and width ranging from 0.4 mm to 1.2 mm, with three per section). There was some variation between inputted sample size and true printed dimensions. **Table S2** contains the input dimensions and resulting true dimensions. All dimensions listed in the text represent the true cross-sectional area of the skeleton. Thick cross bars were used to delineate sections and maintain fracture in one dimension, and had a width of 12 mm, length of 2 mm, and thickness of 0.5 mm. The gauge length was maintained for all samples with a length of 34 mm. An open lattice structure was chosen to enable topological interlocking and improve force transmission between the skeleton and matrix. See supporting information **Figure S1** for detailed structures of the grid, and **Figure S2** for mechanical characterization of the grid. After printing, the grid was washed with deionized water prior to composite fabrication.

4.3 Synthesis of silicone rubber Macro-DN composite

To prepare the reaction vessel, plastic skeletons were placed on a glass plate and surrounded by a 1.5 mm thick silicone spacer. For the silicone system, the silicone rubber precursor solution was prepared by mixing the two silicone components at a mixing ratio of 1:1 in a vacuum mixer (ARV-310, Thinky Corporation). Immediately, the precursor solution was poured into the mold and the mold was placed on a level table for 48 hours to cure the silicone. After that, the sample

was cut into specific dimensions ($l_0 \times w_0 \times t_0$ = 34×12×1.5 mm^3) using a laser cutter (PLS4.75, Universal Laser Systems). A schematic of the sample used in section 2.1 with dimensions can be seen in **Figure S5a**. This results in a sample with 0.5 mm of rubber between the surface and the top of the cross bars, and 1 mm of rubber separating the side from the edge of the cross bars (**Figure S5b** and **Figure S5c**). For the neat silicone rubber (matrix), the samples were prepared at the same formulation and polymerization conditions as those of the composites for the mechanical tests in the absence of the plastic skeletons.

4.4 Synthesis of additional composites

Wood and polystyrene grids were cut to shape using a laser cutter. Combination with silicone rubber occurred following the same procedure as listed above. Samples prepared from natural rubber latex were fabricated using an open cell design with just one glass plate, to allow for evaporation of the latex solution. The composite was dried at room temperature for 3 days.

4.5 Mechanical testing

4.5.1 Tensile tests

Uniaxial tensile tests were performed on the composites, as-prepared silicone rubber (matrix), and the plastic skeletons using a tensile-compressive tester (Instron 5965 type universal testing system). All the samples were stretched along the length direction of the samples at an extension rate of 50 mm/min. Stretch ratio, λ, is defined as l/l_0, where l_0 and l are the length of the specimen before and during elongation, respectively. All stretching experiments were recorded visually with a video camera (Panasonic VX985M). Fracture of the skeleton could be seen visually and appears in the data as a local maximum in force.

The cyclic loading/unloading tensile test for evaluating the energy dissipation ability of the composites was performed by stretching one sample repeatedly with increasing stretch. The

composites and pristine silicone rubber were deformed to strains of ε_x = 0.2 – 1.6 (with increasing intervals of 0.2) at a velocity of 50 mm/min at room temperature. Then, samples were returned to the initial displacement immediately at the same velocity. The energy dissipation was calculated from the hysteresis area, U_{hys} by:

$$U_{hys} = \int_{\varepsilon=0}^{\varepsilon=\varepsilon_x} (\sigma_{load} - \sigma_{unload}) d\varepsilon$$

Where σ_{load} and σ_{unload} are the stress during loading and unloading, respectively.

4.5.2 Interfacial adhesion testing

The pull-out tests were carried out using a tensile tester in order to measure the adhesive strength of the interface between the skeleton and the matrix. Plastic posts (rod-shape skeletons) were 3D printed and embedded to depths of 5, 7, 10 and 16 mm respectively in silicone rubber. The cross-sectional area of the plastic posts was kept constant (0.5 mm × 0.8 mm = 0.4 mm^2) for all the samples. The silicone rubber was fixed to the bottom of a tensile testing machine and the plastic post was fixed to the crosshead, and a pull-out test was conducted at a speed of 50 mm/min. The adhesion strength between the two phases was determined by dividing the maximum value of the force generated between the silicone rubber and the plastic post by the surface area of the plastic post embedded in the silicone rubber. For the fabricated composites, the adhesion strength was calculated by multiplying the adhesive stress with the perimeter of the sacrificial bond, the section interval length, and the number of sacrificial bonds per interval.

SUPPORTING INFORMATION

A comparison of the mechanical properties of skeleton, matrix, and composite; fabrication details of the skeleton; mechanical properties of the skeleton with varying cross-sectional area; influence of skeleton on the stiffness and yield strength of Macro-DN composites; input vs. printed

dimensions of 3D printed skeletons; importance of the number of sacrificial bonds per section; cross-sectional slices of the skeleton highlighting different geometries.

AUTHOR CONTRIBUTIONS

The manuscript was written through contributions of all authors. All authors have given approval to the final version of the manuscript. Conceptualization, D.R.K., J.P.G.; Methodology, D.R.K., T.O., R.T. T.K.; Investigation, T.O., R.T.; Writing – Original Draft, D.R.K.; Writing – Reviewing & Editing, D.R.K., T.O, R.T, J.P.G.; Visualization, D.R.K., R.T.; Supervision, D.R.K., J.P.G.; Funding Acquisition, J.P.G.

CONFLICT OF INTEREST STATEMENT

The authors declare no competing financial interest.

ACKNOWLEDGEMENTS

This work was supported by Japan Society for the Promotion of Science (JSPS) KAKENHI Grant Number 17H06144. DRK acknowledges the Hokkaido University Research Fund Program for Early Career Scientists. JPG acknowledges the Institute for Chemical Reaction Design and Discovery (WPI-ICReDD), established by World Premier International Research Initiative (WPI), MEXT, Japan.

REFERENCES

(1) Creton, C. 50th Anniversary Perspective: Networks and Gels: Soft but Dynamic and Tough. *Macromolecules* **2017**, *50* (21), 8297–8316. https://doi.org/10.1021/acs.macromol.7b01698.

(2) Ramakrishna, S.; Mayer, J. Biomedical Applications of Polymer-Composite Materials: A Review. *Compos. Sci. Technol.* **2001**, *61*, 1189–1224.

(3) Du, X.; Zhou, J.; Shi, J.; Xu, B. Supramolecular Hydrogelators and Hydrogels: From Soft Matter to Molecular Biomaterials. *Chem. Rev.* **2015**, *115* (24), 13165–13307. https://doi.org/10.1021/acs.chemrev.5b00299.

(4) Maeda, S.; Hara, Y.; Sakai, T.; Yoshida, R.; Hashimoto, S. Self-Walking Gel. *Adv. Mater.* **2007**, *19* (21), 3480–3484. https://doi.org/10.1002/adma.200700625.

(5) Wehner, M.; Truby, R. L.; Fitzgerald, D. J.; Mosadegh, B.; Whitesides, G. M.; Lewis, J. A.; Wood, R. J. An Integrated Design and Fabrication Strategy for Entirely Soft, Autonomous Robots. *Nature* **2016**, *536* (7617), 451–455. https://doi.org/10.1038/nature19100.

(6) Markvicka, E. J.; Bartlett, M. D.; Huang, X.; Majidi, C. An Autonomously Electrically Self-Healing Liquid Metal-Elastomer Composite for Robust Soft-Matter Robotics and Electronics. *Nat. Mater.* **2018**, *17* (7), 618–624. https://doi.org/10.1038/s41563-018-0084-7.

(7) Dickey, M. D. Stretchable and Soft Electronics Using Liquid Metals. *Adv. Mater.* **2017**, *1606425* (27), 1–19. https://doi.org/10.1002/adma.201606425.

(8) Okumura, Y.; Ito, K. The Polyrotaxane Gel: A Topological Gel by Figure-of-Eight Cross-Links. *Adv. Mater.* **2001**, *13* (7), 485–487. https://doi.org/10.1002/1521-4095(200104)13:7<485::AID-ADMA485>3.0.CO;2-T.

(9) Noda, Y.; Hayashi, Y.; Ito, K. From Topological Gels to Slide-Ring Materials. *J. Appl. Polym. Sci.* **2014**, *131* (15), 1–9. https://doi.org/10.1002/app.40509.

(10) Sun, J.-Y.; Zhao, X.; Illeperuma, W. R. K.; Chaudhuri, O.; Oh, K. H.; Mooney, D. J.; Vlassak, J. J.; Suo, Z. Highly Stretchable and Tough Hydrogels. *Nature* **2012**, *489* (7414), 133–136. https://doi.org/10.1038/nature11409.

(11) Sun, T. L.; Kurokawa, T.; Kuroda, S.; Ihsan, A. Bin; Akasaki, T.; Sato, K.; Haque, M. A.; Nakajima, T.; Gong, J. P. Physical Hydrogels Composed of Polyampholytes Demonstrate High Toughness and Viscoelasticity. *Nat. Mater.* **2013**, *12* (10), 932–937. https://doi.org/10.1038/nmat3713.

(12) Cordier, P.; Tournilhac, F.; Soulié-Ziakovic, C.; Leibler, L. Self-Healing and Thermoreversible Rubber from Supramolecular Assembly. *Nature* **2008**, *451* (7181), 977–980. https://doi.org/10.1038/nature06669.

(13) Gong, J. P.; Katsuyama, Y.; Kurokawa, T.; Osada, Y. Double-Network Hydrogels with Extremely High Mechanical Strength. *Adv. Mater.* **2003**, *15* (14), 1155–1158. https://doi.org/10.1002/adma.200304907.

(14) Gong, J. P. Why Are Double Network Hydrogels so Tough? *Soft Matter* **2010**, *6* (12), 2583. https://doi.org/10.1039/b924290b.

(15) Brown, H. R. A Model of the Fracture of Double Network Gels. *Macromolecules* **2007**, *40* (10), 3815–3818. https://doi.org/10.1021/ma062642y.

(16) Ducrot, E.; Chen, Y.; Bulters, M.; Sijbesma, R. P.; Creton, C. Toughening Elastomers with Sacrificial Bonds and Watching Them Break. *Science (80-.).* **2014**, *344* (6180), 186–189. https://doi.org/10.1126/science.1248494.

(17) Matsuda, T.; Nakajima, T.; Gong, J. P. Fabrication of Tough and Stretchable Hybrid Double-

Network Elastomers Using Ionic Dissociation of Polyelectrolyte in Nonaqueous Media. *Chem. Mater.* **2019**, *31*, 3766–3776. https://doi.org/10.1021/acs.chemmater.9b00871.

(18) Zhao, X. Multi-Scale Multi-Mechanism Design of Tough Hydrogels: Building Dissipation into Stretchy Networks. *Soft Matter* **2014**, *10* (5), 672–687. https://doi.org/10.1039/c3sm52272e.

(19) Lin, S.; Cao, C.; Wang, Q.; Gonzalez, M.; Dolbow, J. E.; Zhao, X. Design of Stiff, Tough and Stretchy Hydrogel Composites via Nanoscale Hybrid Crosslinking and Macroscale Fiber Reinforcement. *Soft Matter* **2014**, *10* (38), 7519–7527. https://doi.org/10.1039/C4SM01039F.

(20) Visser, J.; Melchels, F. P. W.; Jeon, J. E.; van Bussel, E. M.; Kimpton, L. S.; Byrne, H. M.; Dhert, W. J. A.; Dalton, P. D.; Hutmacher, D. W.; Malda, J. Reinforcement of Hydrogels Using Three-Dimensionally Printed Microfibres. *Nat. Commun.* **2015**, *6* (1), 6933. https://doi.org/10.1038/ncomms7933.

(21) Agrawal, A.; Rahbar, N.; Calvert, P. D. Strong Fiber-Reinforced Hydrogel. *Acta Biomater.* **2013**, *9* (2), 5313–5318. https://doi.org/10.1016/j.actbio.2012.10.011.

(22) Liao, I.-C.; Moutos, F. T.; Estes, B. T.; Zhao, X.; Guilak, F. Composite Three-Dimensional Woven Scaffolds with Interpenetrating Network Hydrogels to Create Functional Synthetic Articular Cartilage. *Adv. Funct. Mater.* **2013**, *23* (47), 5833–5839. https://doi.org/10.1002/adfm.201300483.

(23) Illeperuma, W. R. K. K.; Sun, J.; Suo, Z.; Vlassak, J. J. Fiber-Reinforced Tough Hydrogels. *Extrem. Mech. Lett.* **2014**, *1*, 90–96. https://doi.org/10.1016/j.eml.2014.11.001.

(24) King, D. R.; Sun, T. L.; Huang, Y.; Kurokawa, T.; Nonoyama, T.; Crosby, A. J.; Gong, J. P. Extremely Tough Composites from Fabric Reinforced Polyampholyte Hydrogels. *Mater. Horizons* **2015**, *2* (6), 584–591. https://doi.org/10.1039/C5MH00127G.

(25) Huang, Y.; King, D. R.; Sun, T. L.; Nonoyama, T.; Kurokawa, T.; Nakajima, T.; Gong, J. P. Energy-Dissipative Matrices Enable Synergistic Toughening in Fiber Reinforced Soft Composites. *Adv. Funct. Mater.* **2017**, *27* (9), 1605350. https://doi.org/10.1002/adfm.201605350.

(26) Moutos, F. F. T.; Freed, L. E. LE; Guilak, F. A Biomimetic Three-Dimensional Woven Composite Scaffold for Functional Tissue Engineering of Cartilage. *Nat. Mater.* **2007**, *6* (2), 162–167. https://doi.org/10.1038/nmat1822.

(27) Kazem, N.; Bartlett, M. D.; Majidi, C. Extreme Toughening of Soft Materials with Liquid Metal. *Adv. Mater.* **2018**, *1706594*, 1706594. https://doi.org/10.1002/adma.201706594.

(28) Bartlett, M. D.; Fassler, A.; Kazem, N.; Markvicka, E. J.; Mandal, P.; Majidi, C. Stretchable, High- k Dielectric Elastomers through Liquid-Metal Inclusions. *Adv. Mater.* **2016**, *28* (19), 3726–3731. https://doi.org/10.1002/adma.201506243.

(29) Style, R. W.; Boltyanskiy, R.; Allen, B.; Jensen, K. E.; Foote, H. P.; Wettlaufer, J. S.;

Dufresne, E. R. Stiffening Solids with Liquid Inclusions. *Nat. Phys.* **2015**, *11* (1), 82–87. https://doi.org/10.1038/nphys3181.

(30) Tutika, R.; Zhou, S. H.; Napolitano, R. E.; Bartlett, M. D. Mechanical and Functional Tradeoffs in Multiphase Liquid Metal, Solid Particle Soft Composites. *Adv. Funct. Mater.* **2018**, *1804336* (45), 1804336. https://doi.org/10.1002/adfm.201804336.

(31) Munch, E.; Launey, M. E.; Alsem, D. H.; Saiz, E.; Tomsia, A. P.; Ritchie, R. O. Tough, Bio-Inspired Hybrid Materials. *Science (80-.).* **2008**, *322* (5907), 1516–1520. https://doi.org/10.1126/science.1164865.

(32) Woo, S. L.-Y.; Lee, T. Q.; Abramowitch, S. D.; Gilber, T. W. Structure and Function of Ligaments and Tendons. In *Basic Orthopaedic Biomechanics & Mechano-Biology*; 2005; pp 301–342.

(33) Ateshian, G. A.; Mow, V. C. Basic Orthopaedic Biomechanics and Mechano-Biology. In *Friction, lubrication, and wear of articular cartilage and diarthrodial joints*; 2005; pp 447–494. https://doi.org/9780781739337.

(34) Barthelat, F. Nacre from Mollusk Shells: A Model for High-Performance Structural Materials. *Bioinspir. Biomim.* **2010**, *5* (3), 035001. https://doi.org/10.1088/1748-3182/5/3/035001.

(35) Ritchie, R. O. Natural Materials: Armoured Oyster Shells. *Nat. Mater.* **2014**, *13* (5), 435–437. https://doi.org/10.1038/nmat3956.

(36) Wegst, U. G. K.; Bai, H.; Saiz, E.; Tomsia, A. P.; Ritchie, R. O. Bioinspired Structural Materials. *Nat. Mater.* **2015**, *14* (1), 23–36. https://doi.org/10.1038/nmat4089.

(37) Feng, X.; Ma, Z.; MacArthur, J. V; Giuffre, C. J.; Bastawros, A. F.; Hong, W. A Highly Stretchable Double-Network Composite. *Soft Matter* **2016**, *12* (44), 8999–9006. https://doi.org/10.1039/C6SM01781A.

(38) Shabahang, S.; Tao, G.; Kaufman, J. J.; Qiao, Y.; Wei, L.; Bouchenot, T.; Gordon, A. P.; Fink, Y.; Bai, Y.; Hoy, R. S.; Abouraddy, A. F. Controlled Fragmentation of Multimaterial Fibres and Films via Polymer Cold-Drawing. *Nature* **2016**, *534* (7608), 529–533. https://doi.org/10.1038/nature17980.

(39) Cooper, C. B.; Joshipura, I. D.; Parekh, D. P.; Norkett, J.; Mailen, R.; Miller, V. M.; Genzer, J.; Dickey, M. D. Toughening Stretchable Fibers via Serial Fracturing of a Metallic Core. *Sci. Adv.* **2019**, *5* (2), eaat4600. https://doi.org/10.1126/sciadv.aat4600.

(40) Zhu, F.; Cheng, L.; Wang, Z. J.; Hong, W.; Wu, Z. L.; Yin, J.; Qian, J.; Zheng, Q. 3D-Printed Ultratough Hydrogel Structures with Titin-like Domains. *ACS Appl. Mater. Interfaces* **2017**, *9* (13), 11363–11367. https://doi.org/10.1021/acsami.7b02007.

(41) Takahashi, R.; Sun, T. L.; Saruwatari, Y.; Kurokawa, T.; King, D. R.; Gong, J. P. Creating Stiff, Tough, and Functional Hydrogel Composites with Low-Melting-Point Alloys. *Adv. Mater.* **2018**, *30* (16), 1706885. https://doi.org/10.1002/adma.201706885.

(42) Ragelle, H.; Tibbitt, M. W.; Wu, S. Y.; Castillo, M. A.; Cheng, G. Z.; Gangadharan, S. P.; Anderson, D. G.; Cima, M. J.; Langer, R. Surface Tension-Assisted Additive Manufacturing. *Nat. Commun.* **2018**, *9* (1), 1–10. https://doi.org/10.1038/s41467-018-03391-w.

(43) Li, T.; Chen, Y.; Hu, X.; Li, Y.; Wang, L. Exploiting Negative Poisson's Ratio to Design 3D-Printed Composites with Enhanced Mechanical Properties. *Mater. Des.* **2018**, *142*, 247–258. https://doi.org/10.1016/j.matdes.2018.01.034.

(44) Webber, R. E.; Creton, C.; Brown, H. R.; Gong, J. P. Large Strain Hysteresis and Mullins Effect of Tough Double-Network Hydrogels. *Macromolecules* **2007**, *40* (8), 2919–2927. https://doi.org/10.1021/ma062924y.

(45) Matsuda, T.; Nakajima, T.; Fukuda, Y.; Hong, W.; Sakai, T.; Kurokawa, T.; Chung, U. Il; Gong, J. P. Yielding Criteria of Double Network Hydrogels. *Macromolecules* **2016**, *49* (5), 1865–1872. https://doi.org/10.1021/acs.macromol.5b02592.

(46) Yang, W.; Sherman, V. R.; Gludovatz, B.; Schaible, E.; Stewart, P.; Ritchie, R. O.; Meyers, M. A. On the Tear Resistance of Skin. *Nat. Commun.* **2015**, *6*, 6649. https://doi.org/10.1038/ncomms7649.

(47) Yang, J.; Bai, R.; Suo, Z. Topological Adhesion of Wet Materials. *Adv. Mater.* **2018**, *30* (25), 1–7. https://doi.org/10.1002/adma.201800671.

(48) Steck, J.; Yang, J.; Suo, Z. Covalent Topological Adhesion. *ACS Macro Lett.* **2019**, *8* (6), 754–758. https://doi.org/10.1021/acsmacrolett.9b00325.

(49) Yang, J.; Bai, R.; Li, J.; Yang, C.; Yao, X.; Liu, Q.; Vlassak, J. J.; Mooney, D. J.; Suo, Z. Design Molecular Topology for Wet–Dry Adhesion. *ACS Appl. Mater. Interfaces* **2019**, *11* (27), 24802–24811. https://doi.org/10.1021/acsami.9b07522.

(50) Hubbard, A. M.; Cui, W.; Huang, Y.; Takahashi, R.; Dickey, M. D.; Genzer, J.; King, D. R.; Gong, J. P. Hydrogel/Elastomer Laminates Bonded via Fabric Interphases for Stimuli-Responsive Actuators. *Matter* **2019**. https://doi.org/10.1016/j.matt.2019.04.008.